Proceedings of the ASME 2010 3rd Joint US-European Fluids Engineering Summer Meeting and
8th International Conference on Nanochannels, Microchannels, and Minichannels
FEDSM-ICNMM2010
August 1-5, 2010, Montreal, Canada

FEDSM-ICNMM2010-30191

NUMERICAL STUDY ON DROPLET FORMATION IN A MICROCHANNEL T-JUNCTION USING THE VOF METHOD

Shobeir Aliasghar Zadeh *

Institute of Fluid Mechanics
University of Braunschweig
Bienroder Weg 3, D-38106 Braunschweig, Germany
Email: s.zadeh@tu-bs.de

Rolf Radespiel†

Institute of Fluid Mechanics
University of Braunschweig
Bienroder Weg 3, D-38106 Braunschweig, Germany

ABSTRACT

The liquid-liquid two-phase flow in a T-junction was numerically investigated applying the VOF method and is compared with experimental results. The geometry was generated and meshed using the software Gridgen, and the corresponding equations for the CFD analysis were solved by using the commercial software Fluent (Fluent 12). The generated mesh consists of block-structured grids with hexahedral elements. Water-Glycerol solution (to-be-dispersed phase) and silicone oil (continuous phase) at room conditions are considered as fluids for this work. The effect of various parameters such as flow rate of the phases, width of the channel, viscosity and surface tension on the droplet formation are investigated and compared with available experimental results [1]. The breakup mechanism of droplets in various capillary-number regimes are explained. The numerical results of the length of the generated droplets as a function of the capillary number (varying the flow rate of the continuous phase) are in good agreement with the experimental values, which were measured using the same geometrical and physical properties. Further studies indicate that at a constant flow rate of the continuous phase, the droplet length rises strongly if the flow rate of the disperse phase increases, whereas the relative effects of the viscosity of the continuous phase, and the surface tension between phases on the length of droplets are moderate.

NOMENCLATURE

Ca	Capillary number
C_Q	Volume flow coefficient of disperse phase
C_m	Momentum coefficient
D	Channel depth
f	Body force
h	Channel height
$k(x)$	Curvature of fluid interface
L	Channel length
L_D	Droplet length
p	Pressure
Q_{Wa}	Flow rate of Water-Glycerol
Q_{Si}	Flow rate of Silicone-Oil
Re	Reynolds number of continuous phase
r_a	Axial curvature
r_r	Radial curvature
t	Time
$\vec{v}$	Velocity vector
W	Channel width
α	Volume of fraction
Δp_L	Laplace pressure
ρ	Density
$\Re$	Surface force
σ	Surface tension
μ	Viscosity
CSF	Continuum surface force
VOF	Volume of fraction

INTRODUCTION

The usage of microsystems, which are systems of structures of at least one characteristic dimension in the order of 10

---

[*] Research assistant
[†] Professor

to 100 μm has considerably been increased recently in different areas such as medical science, biotechnology, process engineering and in the field of life-science products. The main reason for such vast usage is the advantage of microstructures with respect to conventional macrostructures such as a better heat transfer due to high surface to volume ratios [2], improvement of mixing quality in mixer processes and better control on microchemical [3] and microbiochemical [4] processes such as separation [5], emulsification, dispersion, membrane microreactor and so on. Hence, the usage of microstructures in comparison with macro devices can greatly increase efficiency and reduce the cost [6], [7]. In this regard, different kinds of microstructures have become of great importance. One of the most important application fields of microsystems is in multiphase flows. In recent years, numbers of researchers have put their interest on the fluid flow behaviour of liquid-liquid and gas-liquid multiphase flows in microchannels and have investigated the formation mechanism of droplets and bubbles.

Generally, some methods for the droplet and bubble generation [8] are known in literature: geometry-dominated breakup [9], [10], crossflow rupturing through microchannel arrays [11], [12], hydrodynamic flow focusing through a small orifice [13], [14], [5] and droplet generation in T-junctions [15], [8], [16], [1]. Many efforts have been made to predict geometric features of droplets by relating them to other relevant parameters such as flow rates, viscosities and the interfacial tension.

In this study our focus is on the droplet generation in one of the simplest multiphase devices, namely the T-junction. First of all we make a brief review on the recent experimental and numerical investigations done on this kind of microstructures. Usage of T-junction geometries for generation of droplets started with the work of Thorsen and his coworkers [17]. In their experiment, they used oil as dispersed phase and water as continuous phase. They explained a model for predicting the droplet size by using the force balance between the shear stresses and the interfacial tension. Nisisako et al. [18] obtained similar results in their work.

Most of all previous studies use the capillary number (*Ca*: see equation 8) in order to describe the flow regimes in multiphase flows, which is the ratio of viscous to interfacial stresses. As a function of increasing Ca, three different regimes for the formation of droplets or bubbles can be identified: squeezing, dripping and jetting. Some authors report in their experimental and numerical investigation on the T-junction that the mechanism of droplet and bubble generation changes if the Ca-number changes: At low-capillary numbers, Garstecki et al. [15] demonstrated that the breakup of droplets or bubbles in a microfluidic T-junction does not occur due to shear stress but due to the pressure drop across the emerging bubble or drop. At high-capillary numbers, Thorsen et al. [17] showed that the dynamics of droplet formation are dominated by the shear stresses that act from the continuous phase on the dispersed phase.

Qian and Lawal [16] numerically investigated gas-liquid multiphase flows in a two-dimensional T-junction geometry using the VOF method. They used air (as dispersed phase) and water (as continuous phase) for their study. They showed that surface tension moderately impacts the slug lengths, whereas the effects of fluid density and viscosity are negligible.

Guo and Chen [19] applied a two-dimensional numerical simulation (using air as dispersed phase and water as continuous phase). Their simulations were carried out using the VOF method and considered *Ca*-numbers ranging from $6.4 \cdot 10^{-4}$ to $1.7 \cdot 10^{-2}$. Their numerical results of droplet lengths in various flow fields from squeezing to dripping agreed well with experimental values.

Van der Graaf et al. [20] used lattice Boltzmann simulations to investigate the droplet size in a three-dimensional T-junction geometry. They showed that lattice Boltzmann is a valid method for predicting the droplet size.

In spite of the numerous experimental studies in the field of multiphase micro T-junction geometries, there are not many three-dimensional numerical works dealing with multiphase flows in micro T-junctions.

In this study we use fully three-dimensional numerical simulation to investigate multiphase (liquid-liquid) flows in a T-junction. As the results from our numerical approach are compared with those from the experimental study done by Oishi et al. [1], the geometrical characteristics of the T-junction and the fluid properties in this research are exactly the same. All simulations were carried out using the VOF method. The objectives of this work are to clarify the mechanisms of droplet generation in various capillary flow regimes. Additionally, influences of different effective parameters such as the width of the microchannel and the surface tension between both fluids as well as effects of the flow rate of both phases and the viscosity of the continuous phase on the formation, buildup and length of the droplets are studied.

GOVERNING EQUATIONS

The governing equations of viscous incompressible Newtonian fluid flows are the continuity and the Navier-Stokes momentum equations:

$$\nabla \cdot \vec{v} = 0 \qquad (1)$$

$$\rho \left(\frac{\partial \vec{v}}{\partial t} + \vec{v} \cdot \nabla \vec{v} \right) = -\nabla p + \mu \nabla^2 \vec{v} + f + \Re \qquad (2)$$

where ρ is the fluid density, $\vec{v}$ is the velocity vector, t is the time, p is the pressure, μ is the fluid dynamic viscosity, f is the body force component and $\Re$ is the body force due to surface tension.

The **VOF (Volume Of Fraction)** formulation relies on the fact that two or more fluids (or phases) are not interpenetrating. The main purpose of the VOF method is to track the interface between two phases. For each phase, a variable is introduced: the volume fraction of the phase in the computational cell α_i (for instance, in two-phases liquid-liquid system the index i shows the continuous liquid phase-1 and the to-be-dispersed liquid phase-2). In each control volume, the volume fraction of all phases sum up to unity. The volume fraction of liquid$-i$ for every non-primary phase is convected in the flow field according to the following equation:

$$\frac{\partial \alpha_i}{\partial t} + \vec{v} \cdot \nabla \alpha_i = 0. \tag{3}$$

For two-phase liquid−liquid systems, if $\alpha_{liquid-1} = 1$ the computational cell is filled with the first phase, whereas it is filled with the second phase if $\alpha_{liquid-1} = 0$. Cells with a value of $\alpha_{liquid-1}$ or $\alpha_{liquid-2}$ between 0 and 1 are considered a part of the phase boundary, where the liquid−1 and liquid−2 interface exists. For the primary phase, the volume fraction is calculated by:

$$\sum_{j=1}^{n} \alpha_j = 1 \tag{4}$$

where n indicates the number of all non-primary phases. If the volume fractions of all phases are known, the density and the dynamic viscosity in each control volume (cell) can be calculated from (e.g. for a two-phase flow):

$$\rho = \alpha_1 \rho_1 + (1 - \alpha_1)\rho_2 \tag{5}$$

$$\mu = \alpha_1 \mu_1 + (1 - \alpha_1)\mu_2 \tag{6}$$

where ρ_1, ρ_2, μ_1 and μ_2 are the densities and the dynamic viscosities of liquid−1 and liquid−2, respectively.

For the calculation of two-phase flows, the interfacial tension force is an important parameter and depends on the interface condition between both phases. The effect of surface tension is taken into account by modeling and adding the force term $\Re$ to the momentum equation Eqn. (2). The model applied in this paper uses the **Continuum Surface Force** (**CSF**) [21] model to describe interfacial surface tension,

$$\Re = \sigma k(x) \nabla \alpha_i \tag{7}$$

where σ is the surface tension between both phases and $k(x)$ is the local mean curvature of the fluid interface ($k(x) = -\nabla \frac{n}{|n|}$, with n as the vector normal to the fluid surface).

MODEL GEOMETRY AND COMPUTATIONAL SETUP

Model for T-junction

A three-dimensional T-shaped microchannel geometry was modeled and studied numerically in this research for the investigation of fluid−fluid two-phase flows. As the results from our numerical approach are compared with those from the experimental study done by Oishi et al. [1], geometrical characteristics of the modeled geometry in this research are exactly the same. The commercial software Gridgen (Gridgen−V15) was used to provide the appropriate geometry and the corresponding meshes.

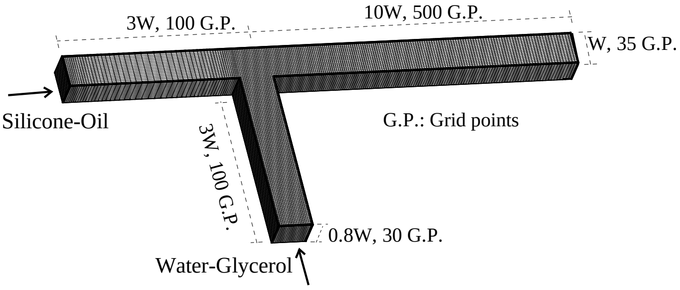

FIGURE 1. SCHEMATIC VIEW OF THE GEOMETRY OF THE T-JUNCTION WITH CORRESPONDING COMPUTATIONAL MESH AND NUMBER OF GRID POINTS IN EACH DIRECTION

A schematic view of this channel is shown in Fig. 1, which comprises the 1300 μm long channel. The length of the channel carrying the water and silicone oil phases is 300 μm, while the mixing channel has a length of 1000 μm. All channels in T-junction configuration have the same rectangular cross-section dimensions, which have a width and height of 100 μm and 80 μm, respectively. The straight main channel carries the continuous fluid (silicone oil), and the discontinuous phase flow (water-glycerol) penetrates into the main channel at the T-shaped junction. At the T-shaped junction the discontinuous phase is deflected toward the outlet of the channel and is transformed into droplets. After the breakup process the generated drops flow within the continuous phase along the straight main channel toward the outlet.

It is noticeable that, as the aspect ratio (the ratio of the width to the height of the channel's cross section) is around unity, there is no possibility to study such channels using a two-dimensional model, which leads to an increased number of grid points and calculation time.

Figure. 1 presents the computational mesh for the aforementioned microchannel. As shown, structured grids using hexahedral elements were used to discretize the model.

Several successive refinement steps of 25 (width) x 20 (height) x $75,300$ (length) cells (coarse), 35 (width) x 30 (height) x $100,500$ (length) cells (medium), and 45 (width) x 40 (height) x $150,700$ (length) cells (fine) were used in the present work. The medium grid was found to be a good compromise between computational accuracy and simulation time. Further increasing the resolution from the medium grid to the fine grid yields no significant changes in the qualitative nature of the simulation results. However, a full refinement study applying eight times the number of grid points was not feasible due to the high computational costs.

Computational setup

The fluid flow inside the T-junction micro multiphase system has a low value of the Reynolds number ($Re = \rho u d_h / \mu \leq 1$, where ρ, μ and d_h are the density, viscosity and the hydraulic diameter of the system, respectively), so the flow can be con-

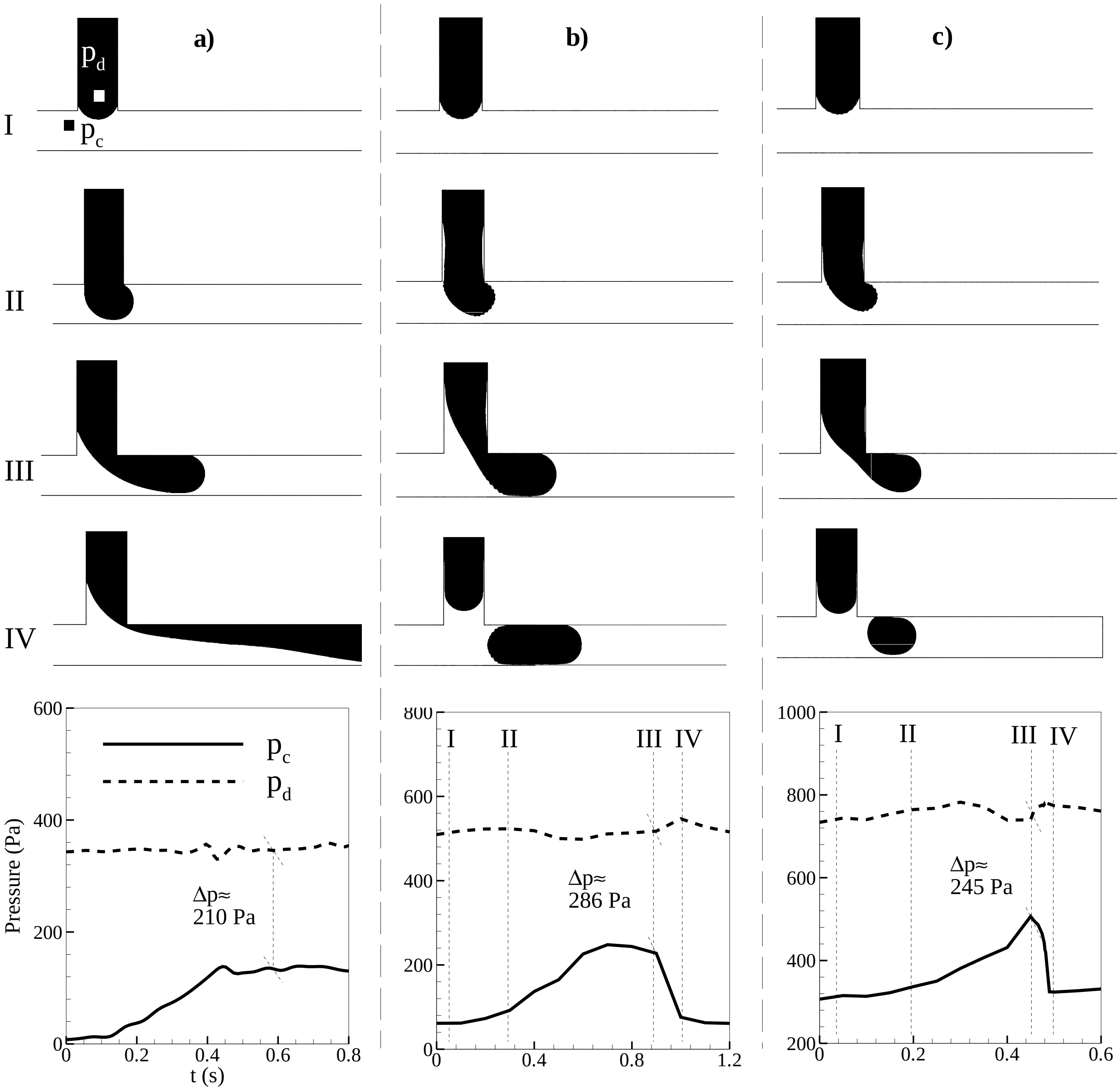

FIGURE 2. TIME EVOLUTION OF A PERIODIC DROPLET GENERATION PROCESS AND ACCORDING PRESSURES IN CONTINUOUS AND DISPERSED PHASE IN THREE CAPILLARY FLOWS: a) VERY-LOW-CAPILLARY NUMBER $Ca = 8.14 \cdot 10^{-4}$, b) LOW-CAPILLARY NUMBER $Ca = 1.6 \cdot 10^{-3}$ AND c) HIGH-CAPILLARY NUMBER $Ca = 8.14 \cdot 10^{-3}$

sidered laminar. A commercial computational fluid dynamics (CFD) code, FLUENT, is employed to numerically simulate the multiphase flow through the T-junction. The differential Navier-Stockes equations (Eqns. 1 and 2) in laminar flow are integrated through the finite-volume method over the control volumes (mesh elements). By applying the Gauss theorem that transforms the volume integrals in surface integrals and by approximating the convection, diffusion and source terms, a system of algebraic equations is gained, which needs to be solved by some iterative method.

In the current study we employ the PISO algorithm [22] (pressure-implicit with splitting of operators) for the pressure-velocity coupling. This scheme is part of the SIMPLE family of algorithms and is based on the higher degree of the approximate relation between the corrections for pressure and velocity. For the pressure interpolation, the PRESTO [23] (pressure staggering option) scheme was applied. The geometric reconstruction scheme was used for the interface interpolation because of its high-accuracy curvature computation. Additionally, in all simulations we adapted the time step in order to keep the Courant number around 1. For this purpose, the simulations were performed applying the adaptive time step option in Fluent. Thereby, the time step may change as the calculation proceeds. If the Courant number during a time step is greater than 1, the size of the next time step is decreased; otherwise, the time step size is increased. Averaging over all simulation runs in the present work yields a mean time step in the order of 10^{-4} s. A maximum of 20 iterations per time step was sufficient to reduce the residuals of all considered transport equations by the order of six. Depending on the velocity of both phases, a total physical timespan between 1 and 2 s was simulated to ensure that several generated droplets could reach the main channel and flow toward the channel outlet.

To close the system of equations the following boundary conditions were used: Dirichlet conditions (uniform velocity inlet for both water and silicone oil phases) and a constant pressure outlet boundary (pressure outlet with the value of ambient pressure at the exit of the main channel) were used at the inlet and outlet of the channel, respectively. No slip boundary conditions were applied at all walls. To consider the effect of surface tension along the interface between water and silicone oil phases, the interface tension was set to 0.0117 N/m, which is value used in the experimental study. In the VOF model used in this study, there is an option to specify the contact angle between the phases and the walls [21]. This so-called dynamic boundary condition results in the adjustment of the curvature of the surface near the wall. In this study, the contact angle was set to 45°.

RESULTS AND DISCUSSION

Mechanism of droplet breakup

According to the previous studies on two-phase flows in T-junctions, three different flow regimes have been established: squeezing, dripping and jetting regime. Most of all previous studies use the capillary number (Ca) in order to describe flow regimes in multiphase flows. Ca is defined as the ratio of shear stresses and the interfacial tension:

$$Ca = \frac{\mu_c v_c}{\sigma}, \tag{8}$$

where μ_c and v_c are the viscosity and the velocity of the continuous phase, respectively, and σ is the surface tension between both phases.

Garstecki et al. [14] focused their study on the mechanism of droplet and bubble formation at small capillary numbers. It was suggested that in small capillary number flows (squeezing regime) the buildup of pressure upstream of the emerging droplet plays the dominant role for the droplet formation. As Ca increases, the formation of droplets transits from squeezing to the dripping regime. Thorsen et al. [17] suggested that the dynamics of droplet formation in the aforementioned dripping regime is dominated by the shear stresses acting on the dispersed phase. With further increase of Ca, the flow regime changes from dripping to jetting. Utada et al. [24] showed that in the jetting regime the droplet formation occurs in the same manner as in the dripping regime: again, shear stresses have the dominant role in the breakup process.

Generally, there are three important forces which participate in the breakup process [14]: The surface tension force (F_σ), the shear-stress force (F_τ) and the force because of the resistance to the continuous phase (F_R). According to the capillary number, the breakup process is the result of the balance of one or two of the latter forces with the surface tension force. The surface tension force is associated with the Laplace-pressure jump (Δp_L) across the phase interface. Δp_L is given from the Young-Laplace equation as follows:

$$\Delta p_L = \sigma(1/r_a + 1/r_r), \tag{9}$$

where r_a and r_r are the axial and radial curvatures, respectively. The Δp_L achieves its maximum value if the curvature at the phase interface becomes minimal. This occurs at the neck of the droplet just before the breakup happens, because at that moment $r_a >> r_r \approx r_{r,min} \approx \frac{h}{2}$ (the radial curvature is bounded by the height of the channel). In our channel with constant values of $\sigma = 0.0117$ N/m and $h = 80$ μm, the maximum of the Laplace-pressure jump almost equals 280 *Pa*.

Figure 2 shows the time sequence of the droplet's generation in four time steps: I) when the tip of the disperse phase enters the main channel, II) when the dispersed phase elongates and grows, III) just before the breakup and IV) just after the breakup of the dispersed phase. All time sequences show the volume of fraction of the disperse phase (black denotes the water phase and white shows the oil phase) along a cross section in the middle of the channel. Using three various velocities for the continuous phase and keeping all other variables constant, according to the Eqn. 8 three flow regimes can be considered : a) very-low-capillary flow ($Ca = 8.14 \cdot 10^{-4}$), b) low-capillary flow ($Ca = 1.6 \cdot 10^{-3}$) and c) high-capillary flow ($Ca = 8.14 \cdot 10^{-3}$).

Generally in all time sequences shown in Fig. 2, with the entrance of the disperse phase into the main channel (I), the stresses acting from the continuous phase cause the disperse phase to be bended toward the outlet of the main channel. Simultaneously, the dispersed phase expands and grows (II and III). At the same time, the interfacial tension attempts to resist the other forces acting on the disperse phase. If sum of the acting forces on the dispersed phase exceeds the maximum Laplace-pressure, droplet breakup happens (sequence IV in Fig. 2-*b*) and *c*)). Otherwise, no breakup happens (sequence IV in Fig. 2-*a*)). Additionally, Fig. 2-*a*), *b*) and *c*) monitor the time history of the pressure evolution at two points in the continuous and in the disperse phase, respectively (point *c* and *d* in Fig. 2-*a*)).

In all three cases, the pressure in the disperse phase remains almost constant while the pressure in continuous phase is increasing during the entrance and penetration of the dispersed phase in the main channel. The reason for this phenomenon is that the disperse phase blocks (totally or partially) the cross section of the main channel which leads to the rise of pressure in

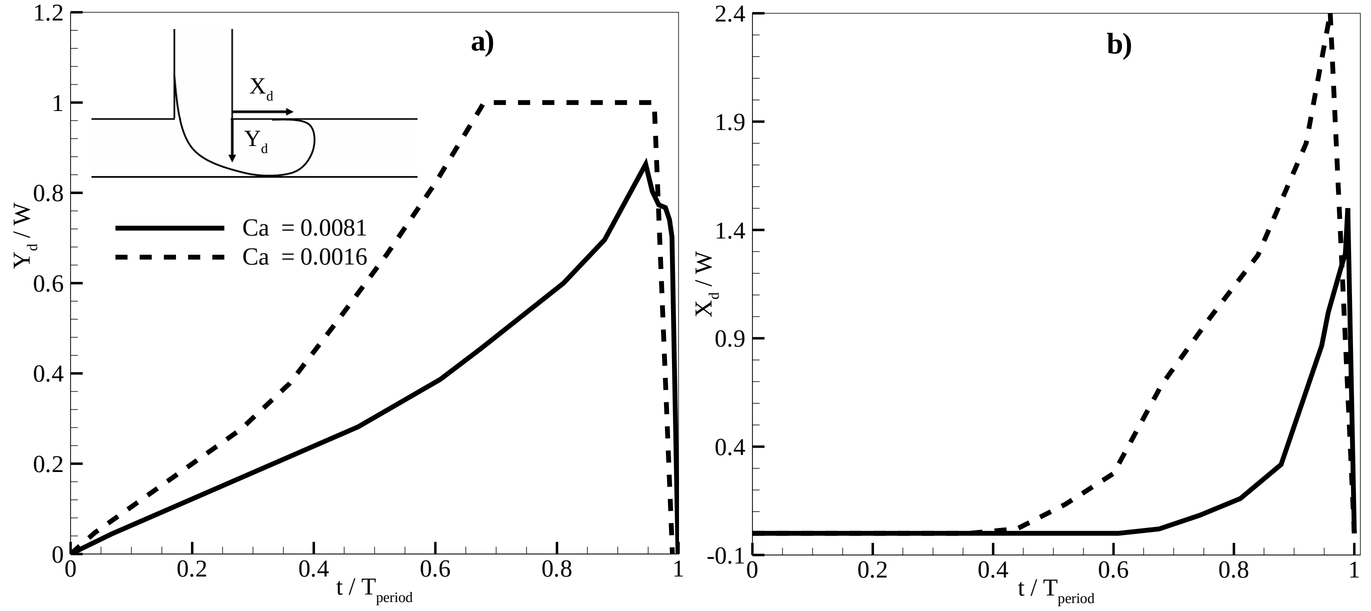

FIGURE 3. TIME HISTORY OF THE DEVELOPMENT OF THE INTERFACE GEOMETRY: a) ELONGATION IN Y_d DIRECTION, b) ELONGATION IN X_d DIRECTION

continuous phase.

First we consider the flow at the very low capillary number (Fig. 2-*a*)): after the disperse phase has blocked the main channel, the pressure difference between the continuous phase and the dispersed phase remains almost constant around 210 *Pa*. This does not exceed the Laplace-pressure and will not be enough for the breakup process ($p_c - p_d < \Delta p_L$). So the disperse and the continuous phase flow together in the main channel and no breakup occurs. Here, the length of the dispersed phase depends on the length of the simulation domain.

In the low-capillary regime (Fig. 2-*b*)), one can see the same process as in the very low-capillary regime, but after the blockage of the main channel, $p_c - p_d \approx 286$ *Pa*, which leads to the breakup of the dispersed phase and the generation of a droplet. After the droplet has separated from the tip, the pressures in both phases jump to the primary conditions and a new period of droplet formation starts.

As the *Ca*-number increases, the flow regime passes from the squeezing to the dripping regime. As shown in (2-*c*)), at the moment of the breakup the pressure difference between both phases is $p_c - p_d \approx 245$ *Pa* $< \Delta p_L$. Although Δp between the both phases does not exceed the Laplace-pressure, breakup occurs. It seems that other forces acting on the disperse phase participate in the breakup process at high-capillary flows. These phenomena can be described as follows: the pressure in the continuous fluid increases while the dispersed phase is growing downstream in the main channel. Because of the relatively higher velocity of the continuous phase, the dispersed phase can only block a part of the cross section of the main channel and a layer of continuous phase develops between the interface and the wall of the channel (gap in the time sequence III in Fig. 2-*c*)). The continuous phase flows through the gap causing shear stresses on the dispersed phase. This force together with the pressure rise due to the partial blockage of the main channel are responsible for the breakup of the dispersed phase. By increasing the capillary number the influence of the shear stress on the dispersed phase becomes more important because the velocity of the continuous phase increases. Thus the dispersed phase blocks the main channel much less and the gap between the dispersed phase and the wall of the channel gets wider.

To make a more precise comparison between the droplet formation in the low- ($Ca = 1.6 \cdot 10^{-3}$) and in the high- ($Ca = 8.14 \cdot 10^{-3}$) capillary flows, the evolution of the interface geometry between the phases in both flow regimes are compared. For this purpose a new coordinate system with two components (X_d and Y_d) is defined, where X_d and Y_d indicate the expansion of the interface of the dispersed phase to the outlet and toward the opposite channel wall (see Fig. 3-*a*)), respectively. Figures 3-*a*) and *b*) illustrate the time history of the interface geometry between both phases. X_d and Y_d are normalized by the width of the channel, while for the normalization of the time, the droplet generation period is used. As shown in Fig. 3-*a*), in both regimes, Y_d increases with time, which means that the dispersed phase progressively blocks the main channel. In the low-capillary flow smaller shear stresses act on the dispersed phase leading to almost complete blockage of the main channel. Then the main channel will stay blocked till the pressure in the continuous phase has sufficiently increased, so that the pressure difference between both phases exceeds the Laplace-pressure (flat segment in the curve related to low-capillary flow). On the other hand, in the high-capillary regime, the higher velocity of the continuous phase causes the disperse phase to only partially block the main channel, and the droplet's breakup happens before the dispersed phase has reached the opposite wall of the main channel (the width of the gap between interface of both phases and the opposite wall of the main channel is ≈ 16 μm).

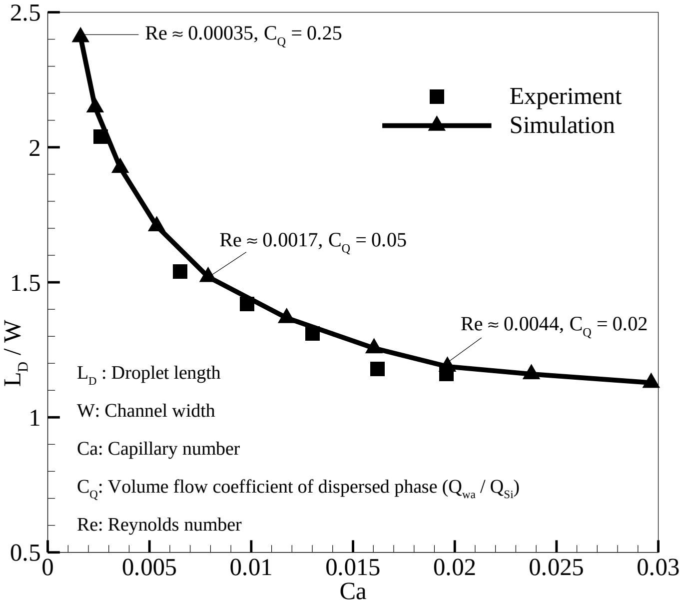

FIGURE 4. COMPARISON BETWEEN THE NUMERICALLY PREDICTED DROPLET LENGTH VALUES AND EXPERIMENTAL RESULTS, $Q_{Water-Glycerol} = 2$ μL/h AND $Q_{Silicone-Oil} = 8$ μL/h to 150 μL/h

Analog to Y_d, the elongation of the disperse phase toward the channel outlet (X_d) is illustrated in Fig. 3-b). Because of the higher shear stresses in the high-capillary flow, the dispersed phase has not much time to be elongated toward the outlet, so that smaller droplets are obtained.

Comparison of numerical simulation with experimental results

The next goal of this work is the comparison between the numerical simulations and the experimental results measured in previous efforts [1]. For this goal, the geometrical and material properties used in this work are the same as applied in the experimental setup. The material properties and flow rates of both phases are shown in Tab. 1.

First, we assume the flow rate of the dispersed phase to be constant ($Q_{Water-Glycerol} = 2$ μL/h), while the flow rate of the continuous phase changes from 8 to 100 μL/h (due to Eqn. 8, the Ca-number depends on the velocity of the continuous phase. Hence, increasing the continuous flow rate leads to the rise of the Ca-number). All other parameters remain constant in all simulations. Post processing of the numerical results is done along the horizontal cross section in the middle of the microchannel. Figure 4 shows the numerical results of the predicted normalized droplet length (L_D/W, where L_D is the length of the droplet and W is the channel width) depending on various Ca-number in comparison with the experimental values. As shown, at low-capillary numbers ($Ca < 0.005$) the droplet length decreases strongly with increasing Ca-number. But in the flow regime at higher capillary numbers ($Ca > 0.005$) the droplet length depends much less on the Ca-number, and in the very high-capillary number regime the droplet length almost remains constant and further increase of the velocity of Silicone-Oil does not lead to any more decrease of the droplet length (for $Ca > 0.0018$ it is $L_D/W \approx 1.17$). Unfortunately, there are no experimental data available for $Ca > 0.02$. But for the Ca-regimes, where both experimental and numerical values are available, very good agreement can be found between the droplet-length values predicted from numerical simulations and experimental measurements.

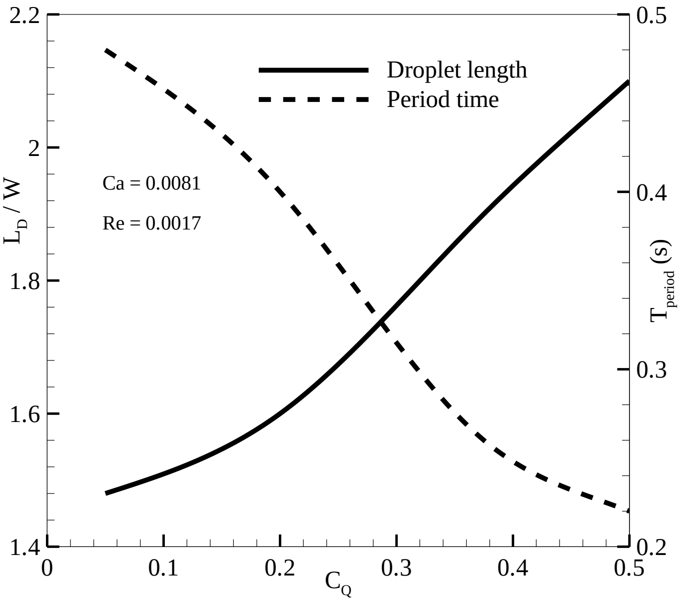

FIGURE 5. EFFECT OF THE VELOCITY OF THE DISPERSED PHASE ON THE DROPLET LENGTH AND TIME PERIOD OF THE DROPLET'S GENERATION, $Q_{Silicone-Oil} = 40$ μL/h AND $Q_{Water-Glycerol} = 2$ to 20 μL/h

TABLE 1. MATERIAL AND FLOW PROPERTIES OF BOTH PHASES

	continuous phase	dispersed phase
working fluid	Silicone oil	Water
Density (kg/m^3)	984	1162
Viscosity ($Pa.s$)	0.0686	0.01058
Surface tension (N/m)	0.0117	
Flow rate ($\mu L/h$)	4 to 150	2

Effect of volume flow of dispersed phase

In another study the effect of the velocity of the dispersed phase is investigated. For this goal, the flow rate of the continuous phase is assumed to be constant, $Q_{Silicone-Oil} =$

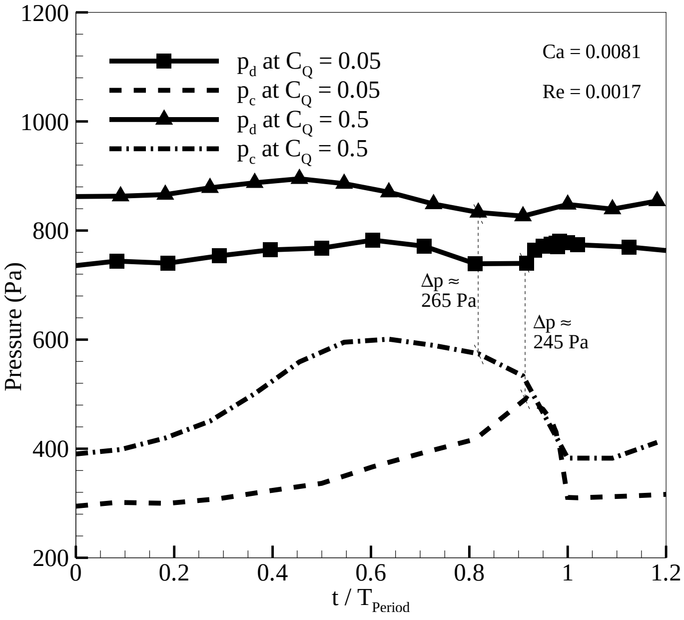

FIGURE 6. TIME EVOLUTION OF PRESSURES IN CONTINUOUS AND DISPERSED PHASE AT $C_Q = 0.05$ AND 0.5

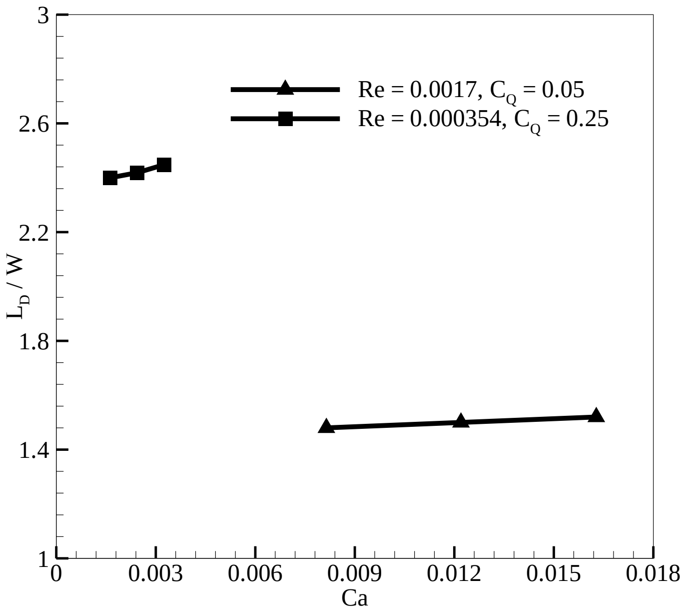

FIGURE 7. EFFECT OF THE SURFACE TENSION ON THE DROPLET LENGTH, $Q_{Water-Glycerol} = 2$ μL/h AND $Q_{Silicone-Oil} =$ 8 μL/h AND 40 μL/h

40 μL/h, while the flow rate of the dispersed phase changes from $Q_{Water-Glycerol} = 2$ μL/h to 20 μL/h. We choose $C_Q = Q_{Water-Glycerol}/Q_{Silicone-Oil}$ as the non-dimensional parameter. The results shown in Fig. 5 clearly show a volume flow effect of the disperse phase. It can be found that at a constant continuous flow rate, the droplet length raise with increasing rate of dispersed phase flow, whereas the time period of the droplet generation decreases if the flow rate of dispersed phase raises.

For a better understanding of these phenomena Fig. 6 shows the normalized time history (for the normalization of the time, the droplet generation period is used) of the pressure evolution in the continuous and in the disperse phase (point c and d in Fig. 2-a)) using two specific flow rates of the disperse phase ($C_Q = 0.05$ and 0.5). As clarified before, at $C_Q = 0.05$ due to the partial blockage of the main channel the continuous phase flows through the gap causing shear stresses on the dispersed phase which leads to the breakup of the droplet. By increasing the disperse phase flow rate (Ca-number remains constant), the disperse phase blocks the main channel much more, the pressure gradient increases, the gap between the dispersed phase and the wall of the channel gets thinner, the effect of shear stresses becomes less important, and breakup happens at a higher pressure difference ($p_c - p_d \approx 265$ Pa).

Other physical effects involved here may be the effect of disperse phase momentum that is represented by the momentum coefficient, $C_m = (\rho \cdot v^2)_{Wa}$ / $(\rho \cdot v^2)_{Si}$, and the disperse Reynolds number, $Re_{Wa} = (\rho \cdot d_h \cdot v/\mu)_{Wa}$. These were not investigated in the present work.

Effect of Capillary number

In the next section of this study, the effect of surface tension on the length of the generated droplets is investigated. For the investigation of the influence of surface tension, the flow rate of the dispersed phased is assumed to be constant ($Q_{Water-Glycerol} = 2$ μL/h). The simulations were done applying two various flow rates for the continuous phase: $Q_{Silicone-Oil} =$ 8 (low-capillary regime) and 40 μL/h (high-capillary regime). Then the simulations were repeated for three different values of surface tensions ($\sigma = 11.7$, 17.5 and 23.4 mN/m). Figure 7 shows the results of the predicted normalized droplet lengths depending on Ca-number at two Reynolds numbers. As shown, the length of the droplet in both flow regimes becomes larger when the surface tension increases. But the gradient of the curve related to the case of the low-capillary regime is slightly higher than in the case of the high-capillary regime. Following Eqn. 9, increasing the surface tension leads to a higher Laplace pressure. In the low-capillary regime, where the pressure difference between the continuous and the dispersed phase plays the dominant role for the droplet breakup, increase of the Laplace pressure causes that higher pressure differences are required for the breakup of the droplet and this leads to the longer droplet. On the other hand, at high-capillary numbers the shear stresses are more important for the breakup process.

Effect of Reynolds number

With the same flow rates setup as used before ($Q_{Water-Glycerol} = 2$ μL/h, $Q_{Silicone-Oil} = 8$ μL/h and 40 μL/h), and varying viscosity (34.3, 68.6, and 137.2 mPa.s), further simulations were carried out to investigate the effect of Reynolds number of the continuous phase on the droplet length. Due to the Eqn. 8, the Ca-number increases with increasing the viscosity of the continuous phase. To consider the effect of Reynolds number at the constant Ca-number, we adjusted

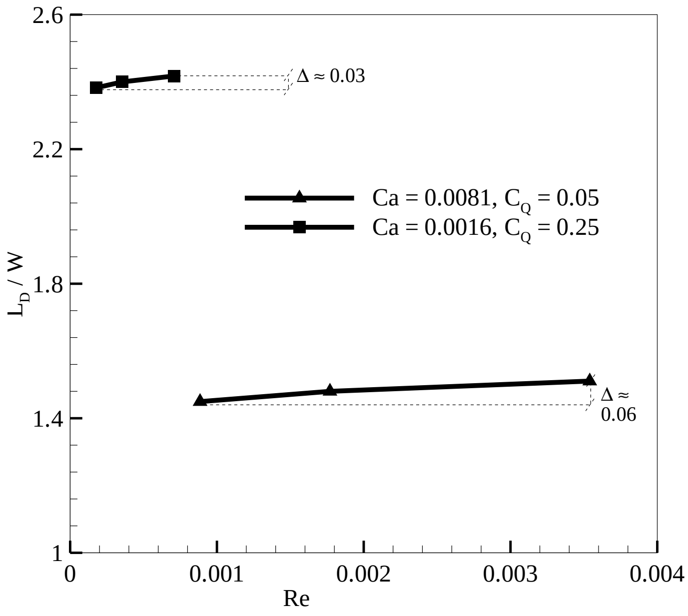

FIGURE 8. EFFECT OF VISCOSITY OF CONTINUOUS PHASE ON THE DROPLET LENGTH, $Q_{Water-Glycerol} = 2$ μL/h AND $Q_{Silicone-Oil} = 8$ μL/h AND 40 μL/h

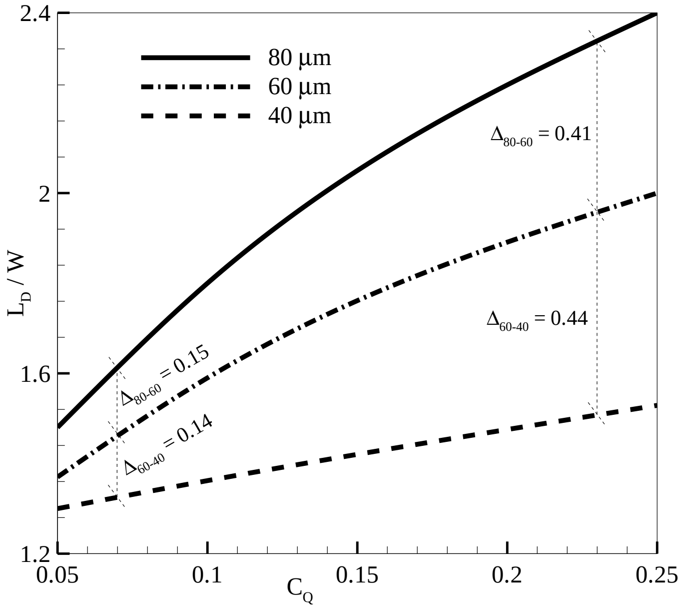

FIGURE 9. EFFECT OF THE WIDTH OF THE MICROCHANNEL ON THE DROPLET LENGTH, $Q_{Water-Glycerol} = 2$ μL/h AND $Q_{Silicone-Oil} = 8$ μL/h TO 40 μL/h

the surface tension, so that the *Ca*-number remains constant for each flow rate of the continuous phase, while the viscosity changes. The results are shown in Fig. 8. It can be found that the droplet length in high-capillary regimes more depends on the viscosity of the continuous phase, as expected.

Channel size sensitivity

The sensitivities to non-dimensional flow parameters as shown above result in important sensitivities of droplet length with respect to channel geometries. This is demonstrated by another set of computations, where the width of the micro T-junction was varied to 40 μm and 60 μm. Both additional channels have the same geometrical properties in any other direction as the original T-junction shown in Fig. 1. We assume the flow rate of the dispersed phase to be constant ($Q_{Water-Glycerol} = 2$ μL/h), while the flow rate of the continuous phase changes from 8 μL/h to 40 μL/h. All other parameters remain constant in all simulations. Post-processing of the numerical results is done along the horizontal cross section in the middle of the microchannel. Figure 9 shows the numerical results of the normalized droplet length (L_D/W) in three T-junction channels depending on various Q_{Si}/Q_{Wa}. As can be found, at all flow rates the droplet length increases as the channel becomes wider. Also, the differences between the predicted droplet lengths Δ at low and high flow rates are shown in Fig. 9. It seems that the dimension of the T-junction microchannel plays a more important role in the low-flow rate regimes, as the difference between the curves decreases from low to the higher flow-rate regimes.

CONCLUSIONS

A series of three-dimensional multiphase flow simulations using the VOF method in a simple T-junction geometry has been performed. The following conclusions can be drawn from the present research:

1. In low-capillary flows the breakup mechanism is dominated by a force balance between the pressure differences between both phases at the phase interface and the Laplace pressure. When the *Ca*-number increases the shear-stress forces acting on the disperse phase become more important for the droplet buildup.
2. The length of droplets predicted by the numerical simulations agree well with the experimental measurements. At a constant flow rate of the disperse phase, the length of the droplets gets smaller as the *Ca*-number increases, and at higher *Ca*-numbers it remains almost constant.
3. At a constant flow rate of the continuous phase, the droplet length rises strongly if the flow rate of the disperse phase increases. The period time of the process decreases with increasing volume flow of the disperse phase.
4. The relative effects of the capillary and Reynolds numbers based on continuous phase properties on the length of droplets are moderate.
5. The computations demonstrate that a significant sensitivity of the droplet length with respect to channel width for given flow rates exists which is a combined effect of Capillary number, volume flow coefficient and Reynolds number.

ACKNOWLEDGMENTS

The authors wish to thank Mr. A. Probst from the Institute of Fluid Mechanics, University of Braunschweig for helpful discussions of the CFD results.

REFERENCES

[1] Oishi, M., Kinishita, H., Fujii, T., and Oshima, M., 2009. "Confocal Micro-PIV Measurement of Droplet Formation in a T-shaped Micro-junction". *Journal of Physics,Conference Series*, ***147***, p. 012061.

[2] Veser, G., 2001. "Experimental and theoretical investigation of H2 oxidation in a high-temperature catalytic microreactor". *Chemical engineering Sience*, ***56***, pp. 1265–1273.

[3] Song, H., Tice, J., and Ismagilov, R., 2003. "A Microfluidic System for Controlling Reaction Networks in Time". *Che. Int. Ed.*, ***42***, pp. 768–772.

[4] Zheng, B., Tice, J., and Ismagilov, R., 2004. "Formation of arrayed droplets of soft lithography and two-phase fluid flow, and application in protein crystallization". *Adv. Mater*, ***16***, pp. 1356–1358.

[5] Fu, A., Spence, C., Scherer, A., Arnold, F., and Quake, S., 1999. "A microfabricated fluorescence-sctivated cell sorter". *Nature Biotechnology*, ***17***, pp. 1109–1111.

[6] Thorsen, T., Maerkl, S., and Quake, S., 2002. "Microfluidic Large Scale Integration". *Science*, ***580***, pp. 580–584.

[7] Kolb, G., and Hessel, V., 2004. "Micro-structured reactors for gas phase reactions". *Chemical engineering*, ***98***, pp. 1–38.

[8] Xu, J. H., Li, S. W., Wang, Y. J., and Luo, G. S., 2006. "Controllable gas-liquid phase flow patterns and monodisperse microbubbles in a microfluidic T-junction device". *Applied Physics Letters*, ***88***, pp. 1–3.

[9] Sugiura, S., Nakajima, M., Iwamoto, S., and Seki, M., 2001. "Interfacial Tension Driven Monodispersed Droplet Formation from Microfabricated Channel Array". *American Chemical Society*, ***17***, pp. 5562–5566.

[10] Kobayashi, S., Nakajima, M., Chun, K., and Kikuchi, Y., 2002. "Silicon Array of Elongated Through-Holes for Monodisperse Emulsion Droplets". *AIChE*, ***48***, pp. 1639–1644.

[11] Xiong, R., Bai, M., and Chung, J., 2007. "Formation of bubbles in a simple co-flowing micro-channel". *Micromechanics and Microengineering*, ***17***, pp. 1002–1011.

[12] Sevilla, A., Gordillo, J. M., and Martinez-Bazan, C., 2005. "Bubble formation in a coflowing airwater stream". *Fluid Mech.*, ***530***, pp. 191–195.

[13] Xu, Q., and Nakajima, M., 2004. "The generation of highly monodisperse droplets through the breakup of hydrodynamically focused microthread in a microfluidic device". *Applied Physics Letters*, ***17***, pp. 3726–3728.

[14] Garstecki, P., Gitlin, I., DiLuzio, W., Whitesidesa, G. M., Kumacheva, E., and Stone, H., 2004. "Formation of monodisperse bubbles in a microfluidic flow-focusing device". *Applied Physics Letters*, ***85***, pp. 2649–2651.

[15] Garstecki, P., Fuerstman, M. J., Stone, H. A., and Whitesides, G. M., 2006. "Formation of Droplets and Bubbles in a Microfluidic T-junction Scaling and Mechanism of Break-Up". *Lab Chip*, ***6***, pp. 437–446.

[16] Qian, D., and Lawal, A., 2006. "Numerical study on gas and liquid slugs for Taylor flow in a T-junction microchannel". *Chemical Engineering Science*, ***61***, pp. 7609–7625.

[17] Thorsen, T., Roberts, R., Arnold, F., and Quake, S., 2001. "Dynamic pattern formation in a vesicle-generating microfluidic device". *Phys. Rev. Lett.*, ***86***, pp. 4163–4166.

[18] Nisisako, T., Torii, T., and Higuchi, T., 2002. "Droplet Formation in a Microchannel Network". *Lab Chip*, ***2***, pp. 24–26.

[19] Guo, F., and Chen, B., 2009. "Numerical Study on Taylor Bubble Formation in a Micro-channel T-junction Using VOF Method". *Microgravity Sci. Technol*, ***21***, pp. 51–58.

[20] van der Graaf, S., Nisisako, T., Schroen, C. G. P. H., van der Sman, R. G. M., and Boom, R. M., 2006. "Lattice Boltzmann Simulations of Droplet Formation in a T-Shaped Microchannel". *Langmuir*, ***22***, pp. 4144–4152.

[21] Brackbill, J., Kothe, D., and Zemach, C., 1992. "A continuum method for modeling surface tension". *Journal of Computational Physics*, ***100***, pp. 335–354.

[22] Issa, R., 1986. "Solution of the implicitly discretized fluid flow equations by operator splitting". *Journal of Computational Physics*, ***62***, pp. 40–65.

[23] Patankar, S. V., 1980. "Numerical Heat Transfer and Fluid Flow". *Hemisphere Publishing Corporation*.

[24] Utada, A. S., Fernandez-Nieves, A., Stone, H. A., and Weitz, A., 2005. "Dripping to jetting transitions in coflowing liquid streams". *Phys. Rev. Lett.*, ***99***, p. 094502.